Dispersive Thermometry with a Josephson Junction Coupled to a Resonator

O.-P. Saira,[1] M. Zgirski,[2] K. L. Viisanen,[1] D. S. Golubev,[1] and J. P. Pekola[1]

[1]*Low Temperature Laboratory, Department of Applied Physics, Aalto University School of Science,*
P.O. Box 13500, 00076 AALTO, Finland
[2]*Institute of Physics, Polish Academy of Sciences, Aleja Lotnikow 32/46, PL-02668 Warsaw, Poland*

We embed a small Josephson junction in a microwave resonator that allows simultaneous dc biasing and dispersive readout. Thermal fluctuations drive the junction into phase diffusion and induce a temperature-dependent shift in the resonance frequency. By sensing the thermal noise of a remote resistor in this manner, we demonstrate primary thermometry in the range of 300 mK to below 100 mK, and high-bandwidth (7.5 MHz) operation with a noise-equivalent temperature of better than 10 μK/$\sqrt{\text{Hz}}$. At a finite bias voltage close to a Fiske resonance, amplification of the microwave probe signal is observed. We develop an accurate theoretical model of our device based on the theory of dynamical Coulomb blockade.

I. INTRODUCTION

An apparently simple coupled system of an ultrasmall Josephson junction and a transmission line resonator exhibits very rich physics which currently attracts a lot of attention. It has been known for a long time that the current-voltage characteristics of such a junction are described by well-developed $P(E)$ theory [1–3], which emphasizes the effect of the electromagnetic environment on the fluctuations of the Josephson phase. This theory has been experimentally verified; see, e.g., Refs. [4–6]. In more recent experiments, the "bright-side" effect, i.e., emission of radiation by the junction into the transmission line, has been detected [7], and the signs of lasing by a single-Cooper-pair box into a resonator have been observed [8]. The experiments have stimulated a series of theory papers that describe, for example, nonlinear quantum dynamics of the system [9,10], emission of entangled photons in two separate resonators [11], antibunching of the emitted photons [12], and the full quantum theory of emitted radiation [13].

In this paper, we demonstrate that depending on bias condition, an ultrasmall Josephson junction can operate either as a sensitive noise detector or as a source of photons. We weakly couple the resonator to the outer transmission line and monitor its resonance frequency and the quality factor via microwave reflection measurements. We show that at zero bias, the shift of the resonance frequency is inversely proportional to temperature, and the junction operates as an ultrasensitive thermometer and noise detector. In this regime, we effectively realize a power-to-frequency transducer. Applying bias voltage V to the junction, we detect amplification of the probe signal close to the resonance condition, where the Josephson frequency $\omega_J = 2eV/\hbar$ matches the fundamental frequency of the resonator ω_r. In this case, the junction may operate as an amplifier or as a source of radiation. We also develop a

high-frequency generalization of the $P(E)$ theory and show that it describes the experiment fairly well in the whole range of bias voltages studied. Our results highlight the unique properties of an ultrasmall Josephson junction and outline future applications as a thermometer or as a general-purpose radiation and noise detector. In particular, we estimate that a thermal photodetector based on this method of temperature sensing can reach photon-resolving energy resolution in the microwave domain.

II. OVERVIEW OF THE EXPERIMENT

A. Sample design

We fabricate a small Josephson junction and couple it to a coplanar waveguide (CPW) resonator that allows simultaneous dc biasing and microwave probing [Figs. 1(a) and 1(b)]. The chip layout and the design philosophy of microwave elements mirror those of superconducting quantum processors [21–23]. In the absence of Josephson dynamics, the fundamental $\lambda/2$ resonance mode is characterized by the resonance frequency $f_r^{(0)} = 5.6681$ GHz, the internal and coupling quality factors $Q_i^{(0)} = 3400$ and $Q_c = 760$, respectively, and impedance $Z_{lc} = (2/\pi)Z_r$, where $Z_r = 30$ Ω is the characteristic impedance of the waveguide. The Josephson element is realized as a planar tunnel junction between an aluminum electrode and a 1-μm-long proximitized Al/Cu/Al superconductor–normal-metal–superconductor (SNS) wire [Fig. 1(c)]. A separate heater line allows local Joule heating of the wire to aid in characterization. Earlier experiments on resonator-coupled tunnel-junction structures have employed thermometry based on quasiparticle transport [24,25], and an initial observation of supercurrent thermometry was reported in Ref. [26]. Details of device fabrication, measurement setup, and microwave readout are presented in the Supplemental Material [15].

024005-1

The sample chip contains another similar device with the resonator 1 GHz lower in frequency. The two device structures can be independently dc biased and read out by frequency multiplexing, and they show similar behavior in the experiments. Here, we mainly discuss the higher-frequency device whose readout resonance has smaller intrinsic loss.

B. Theory

The junction dynamics is described by the equation

$$\int_{-\infty}^{t} dt' Y(t-t') \frac{\hbar \dot{\varphi}}{2e} + I_J = \tilde{I}_{\text{probe}}(t), \qquad (1)$$

where $Y(t) = \int d\omega e^{-i\omega t}/2\pi Z(\omega)$ is the Fourier-transformed admittance of the electromagnetic environment surrounding the junction and including junction capacitance [see Fig. 1(d)], $Z(\omega)$ is the impedance of the environment, I_J is the Josephson current, and $\tilde{I}_{\text{probe}}(t)$ is the current induced by the probe signal. If the junction critical current I_c is high, one should put $I_J = I_c \sin \varphi$ in Eq. (1). However, here we consider the limit $I_c \lesssim 2ek_BT/\hbar$, in which case, applying the theory developed in Refs. [27,28], we find (see the Supplemental Material [15] for details)

$$I_J = \frac{I_c^2}{2e} \int_{-\infty}^{t} dt' e^{-F(t-t')} \sin[K(t-t')]$$
$$\times \sin \left[\varphi(t) - \varphi(t') + \omega_J(t-t') \right]. \qquad (2)$$

Here, $\varphi(t)$ is the high-frequency component of the Josephson phase induced by the combined effect of the probe signal and the resonator. The functions $F(t)$ and $K(t)$ characterize the environment and are defined as follows:

$$F(t) = \frac{4e^2}{\hbar^2} \int \frac{d\omega}{2\pi} S_V(\omega) \frac{1-\cos \omega t}{\omega^2},$$
$$K(t) = \frac{2e^2}{\hbar} \int \frac{d\omega}{2\pi} \frac{Z(\omega)e^{-i\omega t}}{-i\omega + \epsilon}. \qquad (3)$$

In these expressions, $S_V(\omega)$ is the spectral density of voltage fluctuations across the junction, and ϵ is an infinitely small positive constant. In equilibrium, the fluctuation-dissipation theorem is valid, and one finds $S_V(\omega) = \text{Re}[Z(\omega)]\hbar\omega \coth(\hbar\omega/2k_BT)$. In our experiment, the impedance $Z(\omega)$ is dominated by the transmission line resonator [see Figs. 1(a) and 1(d)] and can be formally written as

$$Z(\omega) = i \frac{Z_r}{\pi} \sum_{n=-\infty}^{\infty} \frac{\omega_r^{(0)}}{\omega - n\omega_r^{(0)} + i\gamma_n^{(0)}}, \qquad (4)$$

where $\omega_r^{(0)}$ is the angular frequency of the fundamental ($\lambda/2$) resonance, and $\gamma_n^{(0)}$ is the damping rate of the
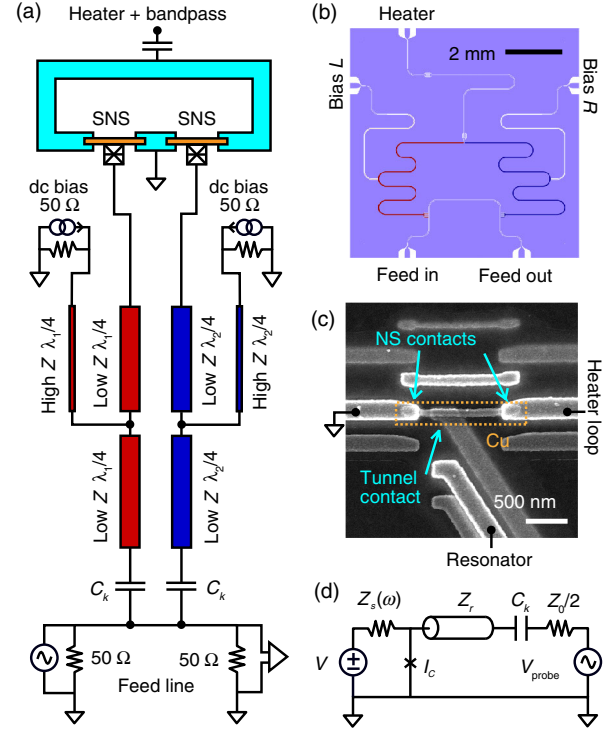

FIG. 1. The studied system. (a) Electrical schematic of the device and essential external components. The left and right halves of the device are functionally equivalent. Coplanar waveguides are used to define microwave resonance modes (at 4.688 and 5.668 GHz for blue and red elements in the illustration, respectively). The combination of low and high characteristic impedance (30 and 125 Ω, respectively) sections of approximately $\lambda/4$ length allow dc biasing while increasing only slightly the losses of the microwave resonance. The resonators couple capacitively to a common feed line for frequency-multiplexed readout. The resonators terminate at small tunnel junctions between an Al electrode and a proximitized Al/Cu/Al (SNS) wire. The two SNS wires are part of the same superconducting loop [14] that couples electrical fluctuations from one wire to the other. Lastly, a microwave line is capacitively connected to a section of the loop and can be used to heat the SNS wires. Detailed wiring is shown in the Supplemental Material [15]. (b) Physical layout of device chip. The CPWs are fabricated from etched Nb on Si substrate. Bandpass filter for the heating line is implemented as an in-line half-wave resonator. (c) Scanning electron micrograph of one of the tunnel junctions fabricated with three-angle shadow evaporation. The disconnected copies of the mask pattern are a by-product of the fabrication method and do not affect the device characteristics. (d) Reduced circuit model used in theory. The dc shunt impedance $Z_s(\omega = 0)$ is denoted by R_s.

nth harmonic mode. One has $\gamma_n^{(0)} = \gamma_{i,n}^{(0)} + \gamma_{c,n}^{(0)}$, where $\gamma_{i,n}^{(0)} = (\omega_r^{(0)} Z_r/\pi) \text{Re}[1/Z_s(n\omega_r^{(0)})]$ is the internal damping, and $\gamma_{c,n}^{(0)} = n^2(\omega_r^{(0)})^3 C_k^2 Z_r Z_0/2\pi$ originates from coupling to the outer transmission line. In the experiment, contributions from up to the second harmonic ($n = 2$) can be observed.

C. Linearized treatment

Linearizing the problem in $\varphi(t)$, we introduce the impedance of the junction

$$Z_J^{-1}(\omega) = i(I_c^2/2\hbar\omega)$$
$$\times [\mathcal{P}(\omega_J) + \mathcal{P}(-\omega_J) - \mathcal{P}(\omega + \omega_J) - \mathcal{P}(\omega - \omega_J)], \quad (5)$$

where the function

$$\mathcal{P}(\omega) = \int_0^\infty dt\, e^{i\omega t} e^{-F(t)} \sin[K(t)] \quad (6)$$

characterizes the high-frequency response of the electromagnetic environment and generalizes the familiar $P(E)$ function. The latter describes only the dc properties of the junction, i.e., its I–V curve. The two functions are related as $\text{Im}[\mathcal{P}(\omega)] = \pi\hbar[P(\hbar\omega) - P(-\hbar\omega)]/2$. Taking the limit $Z_r/R_q \ll 1$ and making use of the small-I_c assumption, we find the modified resonance frequency f_r and the internal damping rate $\gamma_{i,1}$ of the fundamental resonance ($n = 1$) as

$$f_r = f_r^{(0)} + (f_r^{(0)} Z_r/\pi)\text{Im}[Z_J^{-1}(\omega_r^{(0)})], \quad (7)$$

$$\gamma_{i,1} = \gamma_{i,1}^{(0)} - (\omega_r^{(0)} Z_r/\pi)\text{Re}[Z_J^{-1}(\omega_r^{(0)})]. \quad (8)$$

III. ZERO-BIAS OPERATION

At low bias voltages and in the limit of small-signal microwave probing, the voltage dependence of the resonance frequency reduces to a simple Lorentzian form

$$f_r = f_r^{(0)} + \delta + \frac{\Delta f_T}{1 + V^2/V_T^2}, \qquad V_T = \frac{4\pi R_s k_B T}{e R_q}, \quad (9)$$

where $R_s = Z_s(0)$ denotes effective low-frequency shunt resistance, and the other parameters are

$$\Delta f_T = \frac{I_c^2 Z_r}{4\pi^2 k_B T}\left(2\sinh\frac{\pi k_B T}{\hbar\gamma_0}\right)^\alpha,$$

$$\delta = -\frac{\Delta f_T}{1 + \hbar\gamma_0/2eV_T},$$

$\alpha = 8e^2 R_s/2\pi\hbar$, and $\gamma_0 = Z_r\omega_r^{(0)}/\pi R_s$. To arrive at Eq. (9), we assume $\hbar\gamma_0 \gg k_B T$, and the limit of classical phase fluctuations $R_s(0), Z_r, Z_0 \ll R_q = h/e^2 = 25.8$ kΩ. Both conditions are satisfied in our experiment.

In the experiment, the resonance line displays a clear temperature [Fig. 2(c)] and bias dependence. In Fig. 2(a), we analyze the experimental low-bias part of frequency-voltage dependence, which indeed has the Lorentzian form. The width of the Lorentzian is proportional to the temperature at $T \gtrsim 70$ mK [Fig. 2(b)]. Comparing the
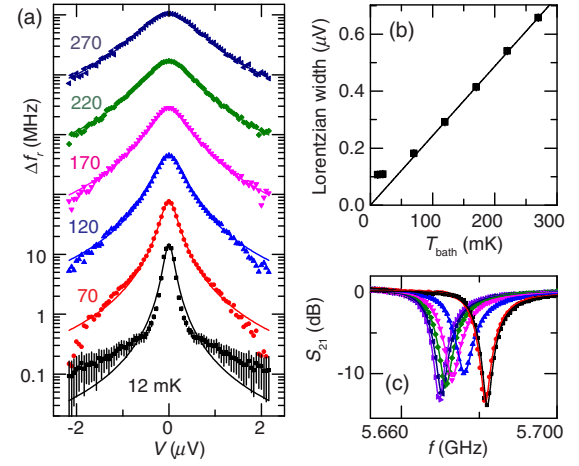

FIG. 2. Primary thermometry in phase diffusion regime of the Josephson junction. (a) Measured change in the resonance frequency as a function of bias voltage at different bath temperatures relative to a baseline (approximately 5.668 GHz) established from Lorentzian fits (lines). Above 12 mK, data are vertically offset by one order of magnitude per temperature point for clarity. (b) The width of the zero-bias feature as a function of the bath temperature and a linear fit with zero intercept. (c) Resonance lines at $V = 0$ at different bath temperatures. Marker symbols (data) and line color (fits) indicate the temperature as in panel (a).

experimental temperature dependence of the width with Eq. (9), we determine the low-frequency shunt resistance $R_s = 57.4$ Ω. By design, the shunt resistance is given by the external bias resistor (nominally, 50 Ω) plus any effective in-line dc resistance including the SNS wire and contacts (approximately 4 Ω for Cu in normal state). The deviation from the linear dependence at lowest temperatures is due to two independent mechanisms. When the condition $I_c < 2ek_B T/\hbar$ is violated, our model no longer applies, and a supercurrent feature with a width close to $I_c R_s$ emerges instead. In addition to this, insufficient thermalization can result in saturation of sample temperature. With the linear scaling established earlier, the minimum observed width corresponds to a temperature of 44 mK [29].

One can similarly work out the approximate form of the quality factor at low bias voltage. The result reads

$$\frac{1}{Q_i} = \frac{1}{Q_i^{(0)}} + \frac{2eI_C^2 Z_r^2}{\pi^2 \hbar\omega_r^{(0)} V_T}\left(2\sinh\frac{\pi k_B T}{\hbar\gamma_0}\right)^{8R_s/R_q}\frac{1}{1 + V^2/V_T^2}. \quad (10)$$

Here we assume that the thermal linewidth significantly exceeds the damping rate of the fundamental resonance [15]. This condition is satisfied in our experiment.

IV. FINITE-VOLTAGE RESONANCES

In Figs. 3(a) and 3(b) we show, respectively, the resonance frequency f and the internal quality factor Q_i as a function of the bias voltage applied to the junction. The
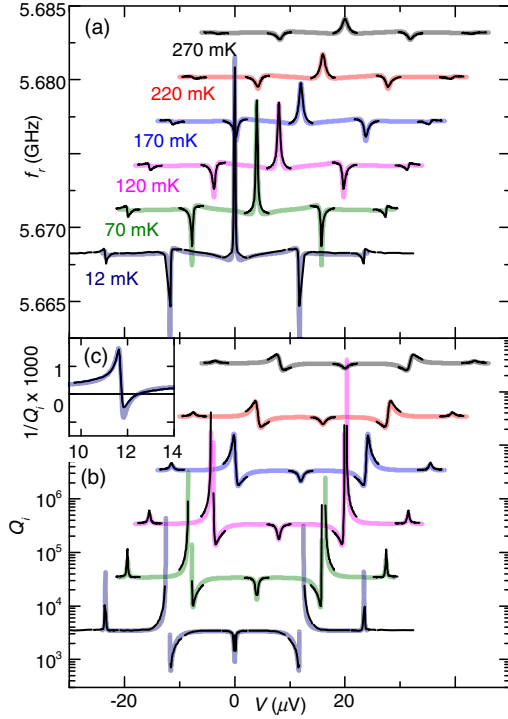
FIG. 3. Bias dependence of microwave response together with detailed theory. (a), (b) Resonance frequency and quality factor, respectively, versus bias voltage at different temperatures. Data at temperatures other than 12 mK are offset for clarity. Thin lines are experimental data, thick faded lines are fits with full small-signal theory. We use $R_s = 57.4\ \Omega$ and choose the critical currents $I_c = 3.25, 3.21, 3.14, 3, 2.7, 2.42, 2.06$ nA and for the bath temperatures $T = 12, 20, 70, 120, 170, 220,$ and 270 mK, respectively. The noise temperature sensed by the junction is set in accordance with the width of the Lorentzian zero-bias feature; cf. Fig. 2(b). The inset (c) highlights a region of negative Q_i observed at base temperature as predicted by theory.

experimental data are fitted with the temperature-dependent critical current I_c as the only free parameter. (Refer to the Supplemental Material [15] for a comparison of I_c values determined with different methods and for theory expressions covering full bias range.) It is interesting that the internal quality factor Q_i becomes negative at bias voltages close to $\hbar\omega_r^{(0)}/2e$ and at a sufficiently low temperature [Fig. 3(c)]. In this regime, the junction pumps energy into the resonator and amplifies the probe signal. Previously, emission from the junction has been detected under similar conditions [7]. The theory predicts that the internal damping becomes negative at $T < T^* = I_c^2 Z_r Q_i^{(0)}/4\pi k_B \omega_r^{(0)}$ and for bias voltages in the range

$$\left| V - \frac{\hbar\omega_r^{(0)}}{2e} - \frac{2eR_s k_B T^*}{\hbar} \right| < \frac{2eR_s k_B \sqrt{T^{*2} - T^2}}{\hbar}. \quad (11)$$

Taking $I_c \approx 3$ nA, we estimate the threshold temperature to be $T^* \approx 150$ mK. Experimentally, the threshold

temperature lies between 120 and 170 mK based on data shown in Fig. 3(b). Although the condition $Q_i < 0$ indicates the generation of microwave power by the junction, it does not imply $|S_{21}| > 1$ in the two-port feed-line configuration employed in our experiment. For that, a stricter condition $1/Q_i + 1/2Q_c^{(0)} < 0$ needs to be met, which occurs theoretically at $T < T^*/(1 + Q_i^{(0)}/2Q_c^{(0)}) \approx 45$ mK and is not realized in the experiment. In earlier work [30], a one-port device based on this principle has been operated as a reflection amplifier at 2.8 GHz.

V. NONLINEAR OPERATION

A. High-power readout

Here, we relax the assumption $|\varphi| \ll 1$ to describe the response to strong microwave probing. High-power probing is relevant for optimizing the noise-equivalent temperature, although overheating of the sample can impose a stricter limit to probing power than the nonlinearity of Josephson dynamics. In a two-port feed-line configuration employed in the experiment, the amplitude of high-frequency phase modulation ϕ_1 is related to the incident probe power P_{in} at probe frequency f_p as

$$\phi_1 = \frac{4Q}{eR_q f_r} \sqrt{\frac{2Z_r P_{in}}{\pi Q_c \left(1 + 4Q^2 \frac{(f_p - f_r)^2}{f_r^2}\right)}}, \quad (12)$$

where $Q^{-1} = Q_c^{-1} + Q_i^{-1}$. Denoting by $\tilde{f}$ and $\tilde{Q}_i$ the power-dependent expressions for the resonance frequency and internal quality factor, respectively, we find the relations

$$\tilde{f}_r - f_r^{(0)} = [J_0^2(\phi_1) - J_1^2(\phi_1)](f_r - f_r^{(0)}), \quad (13)$$

$$\frac{1}{\tilde{Q}_i} - \frac{1}{Q_i^{(0)}} = [J_0^2(\phi_1) - J_2^2(\phi_1)]\left(\frac{1}{Q_i} - \frac{1}{Q_i^{(0)}}\right), \quad (14)$$

where the J_n are Bessel functions of the first kind, and the small-signal f_r and Q_i are evaluated according to Eqs. (4) and (5), respectively. An experimental power sweep performed at zero bias and at the base temperature of the cryostat (13 mK) [Fig. 4(a)] indeed reveals Bessel-type oscillations of the resonance frequency. Solution of the circuit model with ϕ_1-dependent $\tilde{f}_r$ and $\tilde{Q}_i$ reproduces the data well [Fig. 4(b)] including fine structure that appears with off-resonant probing at large power.

The nonlinearity of the model can result in multivalued solutions for certain combinations of low temperature, large I_c, and large probing power. We do not observe hysteretic or bistable behavior in the experiment. Physically, it is likely that large probing power locally heats up parts of the sample or the surrounding circuitry, raising the effective temperature. It is, in principle, possible to include a thermal
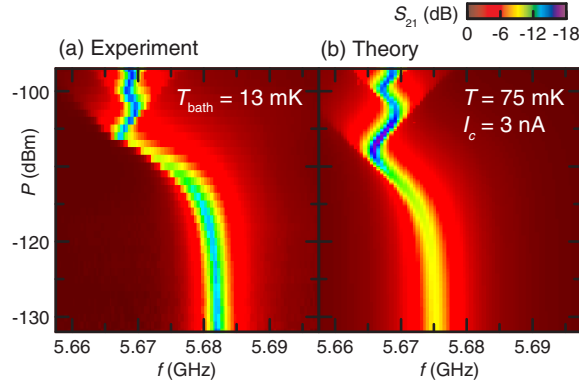
FIG. 4. Effect of large probe power on resonance line at zero bias. The experimental data (left) are obtained at the base temperature of the cryostat (13 mK). The theory data are calculated using a nonlinear model that describes the effect of large phase oscillations on effective junction dynamics. In the simulation, we use an artificially elevated constant temperature (75 mK) for the electromagnetic environment to suppress hysteresis in the model.

balance in the model and solve it in a self-consistent manner. Here, we explain the high-power response by using a constant elevated temperature (75 mK) throughout the simulation. Good agreement with the constant-temperature simulation shows that the present design is not severely overheated even at an incident probing power of −100 dBm.

B. Local heating

In an idealized description of our device, the Josephson element does not have an internal temperature of its own. Instead, the observed temperature dependence stems from fluctuations of the electromagnetic environment. Localized Joule heating or electronic cooling of the SNS wire will generally drive the system to a quasiequilibrium state with independent electron and environment temperatures [31]. We demonstrate sensitivity to the local electron temperature by modulating the wire temperature with either cw microwave heating or by voltage biasing the other tunnel junction that is otherwise unused in the experiment (data are shown in the Supplemental Material [15]). The data are consistent with a model where the cryostat sets the temperature of the electromagnetic environment by thermalizing the cold bias resistor, and the wire temperature is probed through its effect on the I_c of the junction. Here, the temperature dependence follows from that of proximity superconductivity in diffusive metallic weak links [32]. Optimized detectors based on this mode of operation have been explored in detail in earlier works by Govenius *et al.* [33,34].

VI. SENSITIVITY AND NOISE

To evaluate the suitability of this thermometer for calorimetric and bolometric experiments [35], we characterize the sensitivity of the temperature readout with cw
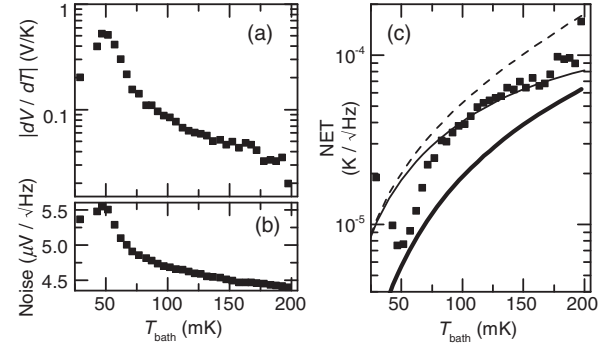

FIG. 5. Sensitivity and noise of temperature readout with quadrature detection. (a) Voltage responsivity at the output of the readout chain using heterodyne detection with $f_{\mathrm{IF}} = 1$ MHz. Magnitude of the complex quantity is shown. (b) Mean spectral density of voltage noise in the frequency band from 10 kHz to 0.3 MHz. (c) Noise-equivalent temperature inferred from (a) and (b) including a $\sqrt{2}$ gain from ideal homodyne detection (experiment, symbols) with superimposed theoretical models: Constant probing power in the small-signal regime (dashed line). Same with responsivity enhancement from explicit temperature dependence of I_c (thin solid line). Minimum achievable NET with optimized probing power at each temperature from a nonlinear model (thick line).

microwave probing at zero bias with phase-sensitive heterodyne readout. Despite conceptual similarities with noise thermometry employing superconducting quantum-interference-device readout [36], our device indicates the temperature directly through a change in the phase of the probe signal instead of relying on power detection with room-temperature electronics. To scan rapidly the parameter space of possible combinations of probing frequency and power, we study the single-shot detection fidelity of discrete heating pulses (1-μs duration, 0.8-pW nominal power) using only the thermometer readout. An optimum is found at 5.671 GHz with a nominal incident power of −118 dBm at the sample box. Next, during a bath temperature sweep up to 200 mK, we record the cw quadrature voltage amplitudes V_I, V_Q and the full noise spectrum of the quadrature readout. We evaluate numerically the voltage responsivity $dV/dT = \sqrt{(dV_I/dT)^2 + (dV_Q/dT)^2}$ corresponding to homodyne detection with optimal phase [Fig. 5(a)]. Similarly, the noise-equivalent temperature (NET) for homodyne detection is $V_{\mathrm{rms}}(dV/dT)^{-1}/\sqrt{2}$, where V_{rms} is the voltage noise level in one quadrature [Figs. 5(b) and 5(c)]. Using the small-signal theory and sample parameters determined earlier, we can reproduce the observed NET values for temperatures higher than 75 mK. We include the responsivity enhancement from the weak temperature dependence of I_c in the model. Comparing the results to a calculation with $\partial I_c/\partial T = 0$, we find that inductance and noise contributions to responsivity are equal at 200 mK, with

the inductance modulation losing its significance below 100 mK. For the theoretical NET calculation, we assume a total power loss of 11 dB from cabling between generator output and the cold amplifier, and amplifier-limited system noise with $T_{\text{noise}} = 2$ K (as per preamplifier specifications). These quantities cannot be independently determined within a linearized model. The origin of the temperature-dependent component of readout noise that follows the shape of the responsivity curve is unknown. The low-frequency resonator is measured simultaneously in an identical manner, and the noise level is found to be constant within 0.5%. We estimate the power dissipated at the sample (P_{diss} including shunt resistors) as ηP_{in}, where P_{in} is the incident probing power and $\eta = 2Q_c Q_i/(Q_c + Q_i)^2$ using modeled values for Q_c and Q_i. The loss fraction η is smaller than 0.5 at all temperatures, resulting in total dissipation less than 0.8 fW [37]. Finally, using the theory for high-power readout presented in Sec. V A, we evaluate the lowest achievable NET when overheating of the sample is neglected [Fig. 5(c), thick line].

VII. OUTLOOK

Small power dissipation, submicrosecond temporal resolution, and good sensitivity at sub-100-mK temperatures make this type of a thermometer a promising candidate for calorimetric experiments [35]. In a nanocalorimeter implementation [26], the external macroscopic bias resistor will be replaced with a metallic or semiconducting nanowire with similar resistance but minimal volume. In a calorimeter device, it is critical to consider the trade-off between the thermometer sensitivity and the power dissipation induced by the thermometer readout. One can formalize this trade-off by writing the NET (units $K/\sqrt{\text{Hz}}$) explicitly in terms of P_{in}. For a dispersive thermometer, the general result

$$\text{NET} = \frac{f_r Q_c}{4Q^2} \left(\frac{df_r}{dT}\right)^{-1} \sqrt{\frac{k_B T_{\text{noise}}}{P_{\text{in}}}} \quad (15)$$

follows from linearized circuit theory assuming one-port reflection measurement and readout noise that is described by the system noise temperature T_{noise}. As long as the responsivity df_r/dT does not explicitly depend on Q_c, the choice $Q_c = Q_i$ is optimal. For a pure reflection measurement, this choice implies $P_{\text{in}} = P_{\text{diss}}$ at resonance. It is possible to derive simple expressions describing our Josephson thermometer by substituting the linear-response formulas of Eqs. (9) and (10) with $V = 0$ and assuming $R_s/R_q \ll 1$. One has

$$\text{NET} = \frac{2T Z_r}{\pi R_s} \sqrt{\frac{k_B T_{\text{noise}}}{P_{\text{in}}}}, \quad (16)$$

to the first order in $Z_r/\pi R_s$. Working from the above relation, one can estimate the expected energy resolution of a

calorimeter under quite general assumptions (see the Appendix for details) about the temperature dependence of the heat capacity ($C_{\text{th}} \propto T^a$) and the thermal link of the calorimeter platform ($G_{\text{th}} \propto T^{b-1}$) as

$$\delta E \approx 2\sqrt{a + b + 1}\sqrt{C_{\text{th}} T k_B T_{\text{noise}}}\frac{Z_r}{\pi R_s}. \quad (17)$$

Note that the validity of Eq. (9) requires the fraction $Z_r/\pi R_s$ to be larger than $k_B T/\hbar\omega_r$. For a practical example, we consider a small metallic absorber ($C_{\text{th}} = 300 k_B$, $a = 1$) on a suspended platform with quantized phononic heat conductance ($b = 2$; see Ref. [36]) at a temperature of 20 mK, microwave probe at $\omega_r = 2\pi \times 5$ GHz, and a readout chain approaching the standard quantum limit $k_B T_{\text{noise}} = \hbar\omega_r$, which results in an estimated energy resolution of 9.6 GHz $\times h$.

In conclusion, we construct a power-to-frequency transducer based on a small Josephson junction and demonstrate sensitive high-bandwidth thermometry at sub-100-mK temperatures. We also develop a theoretical model based on strong environmental fluctuations that describes the measurements within its expected range of validity. Good performance and versatility of the approach suggest it can find use in a wide range of experiments requiring sensitive thermometry, calorimetry, or noise detection. Our results also hint at the possibility of further performance gains in designs with large I_c and/or R_s, whose analysis, however, requires an improved theoretical model.

APPENDIX: CALORIMETER OPTIMIZATION

We consider a generic calorimeter platform that is described by the model equations

$$\delta E = \text{NET}\sqrt{C_{\text{th}} G_{\text{th}}},$$
$$C_{\text{th}} = AT^a,$$
$$G_{\text{th}} = \frac{\partial \dot{Q}}{\partial T},$$
$$\dot{Q} = B(T^b - T_{\text{bath}}^b),$$
$$\text{NET} = f(P_{\text{diss}}, T)$$

subject to steady-state thermal balance

$$P_{\text{diss}} - \dot{Q} = 0, \tag{A1}$$

where T and T_{bath} denote the temperature of the calorimeter and its surrounding thermal bath, respectively, δE is the energy resolution, C_{th} is the heat capacity of the calorimeter, G_{th} is its linearized heat conductance at the operation point, $\dot{Q}$ describes the steady-state heat flow between the calorimeter and its surroundings, a, b are numbers and A and B numerical constants describing the thermal properties of the calorimeter, and f describes the sensitivity of the thermometer as a function of the steady-state dissipation P_{diss} and T_{el}. The choice of the readout power (or, equivalently, P_{diss}) influences the steady-state operation temperature T, and, consequently, δE through the temperature dependence of G_{th} and C_{th}.

Furthermore, if one has

$$f = F P_{\text{diss}}^{-1/2} T^c, \tag{A2}$$

with F a numerical constant and c a number, the problem can be solved through the introduction of a Lagrange multiplier. Note that Eq. (16) describing our thermometer is of this form. One finds

$$P_{\text{diss}}^* = (a + b + 2c - 1)^{-1} T^* G_{\text{th}}^* \tag{A3}$$

and

$$\delta E^* = (a + b + 2c - 1)^{1/2} F(T^*)^{c-1/2} \sqrt{C_{\text{th}}^*}, \tag{A4}$$

where the superscript $*$ denotes quantities calculated at the optimum steady-state (P_{diss}, T) operation point. In practice, one can evaluate Eq. (A4) with $T_{\text{bath}} = T^*$ to approximate the energy resolution, as the optimal probing power does not raise the absorber temperature significantly.

---

[1] D. V. Averin, Yu. V. Nazarov, and A. A. Odintsov, Incoherent tunneling of the Cooper pairs and magnetic flux quanta in ultrasmall Josephson junctions, Physica (Amsterdam) **165B–166B,** 945 (1990).

[2] G. L. Ingold and Yu. V. Nazarov, in *Single Charge Tunneling*, NATO ASI Series B, Vol. 294 edited by H. Grabert and M. H. Devoret (Plenum, New York, 1992), pp. 21–107.

[3] G. L. Ingold, H. Grabert, and U. Eberhardt, Cooper-pair current through ultrasmall Josephson junctions, Phys. Rev. B **50,** 395 (1994).

[4] T. Holst, D. Esteve, C. Urbina, and M. H. Devoret, Effect of a Transmission Line Resonator on a Small Capacitance Tunnel Junction, Phys. Rev. Lett. **73,** 3455 (1994).

[5] A. Steinbach, P. Joyez, A. Cottet, D. Esteve, M. H. Devoret, M. E. Huber, and John M. Martinis, Direct Measurement of the Josephson Supercurrent in an Ultrasmall Josephson Junction, Phys. Rev. Lett. **87,** 137003 (2001).

[6] Yu. A. Pashkin, H. Im, J. Leppkangas, T. F. Li, O. Astafiev, A. A. Abdumalikov, Jr., E. Thuneberg, and J. S. Tsai,

[7] M. Hofheinz, F. Portier, Q. Baudouin, P. Joyez, D. Vion, P. Bertet, P. Roche, and D. Esteve, Bright Side of the Coulomb Blockade, Phys. Rev. Lett. **106,** 217005 (2011).

[8] F. Chen, J. Li, A. D. Armour, E. Brahimi, J. Stettenheim, A. J. Sirois, R. W. Simmonds, M. P. Blencowe, and A. J. Rimberg, Realization of a single-Cooper-pair Josephson laser, Phys. Rev. B **90,** 020506(R) (2014).

[9] V. Gramich, B. Kubala, S. Rohrer, and J. Ankerhold, From Coulomb-Blockade to Nonlinear Quantum Dynamics in a Superconducting Circuit with a Resonator, Phys. Rev. Lett. **111,** 247002 (2013).

[10] B. Kubala, V. Gramich, and J. Ankerhold, Non-classical light from superconducting resonators coupled to voltage-biased Josephson junctions, Phys. Scr. **T165,** 014029 (2015).

[11] A. D. Armour, B. Kubala, and J. Ankerhold, Josephson photonics with a two-mode superconducting circuit, Phys. Rev. B **91,** 184508 (2015).

[12] J. Leppkangas, M. Fogelstrm, A. Grimm, M. Hofheinz, M. Marthaler, and G. Johansson, Antibunched Photons from Inelastic Cooper-Pair Tunneling, Phys. Rev. Lett. **115,** 027004 (2015).

[13] J. Leppäkangas, M. Fogelström, M. Marthaler, and G. Johansson, Correlated Cooper pair transport and microwave photon emission in the dynamical Coulomb blockade, Phys. Rev. B **93,** 014506 (2016).

[14] Weak flux modulation with a global coil is observed. For the higher, more sensitive resonator, the peak-to-peak amplitude is 2 MHz at zero bias. In all subsequent experiments, the flux setting for the largest frequency shift is used.

[15] See Supplemental Material at http://link.aps.org/supplemental/10.1103/PhysRevApplied.6.024005, which includes Refs. [16–20], for extensive derivations, details of experimental methods, and supporting data.

[16] R. Simons, *Coplanar Waveguide Circuits, Components, and Systems* (Wiley, New York, 2001).

[17] R. Barends, Ph.D. thesis, Delft University of Technology, 2009.

[18] K. Geerlings, S. Shankar, E. Edwards, L. Frunzio, R. J. Schoelkopf, and M. H. Devoret, Improving the quality factor of microwave compact resonators by optimizing their geometrical parameters, Appl. Phys. Lett. **100,** 192601 (2012).

[19] M. Nahum, T. M. Eiles, and J. M. Martinis, Electronic microrefrigerator based on a normal-insulator-superconductor tunnel junction, Appl. Phys. Lett., **65,** 3123 (1994).

[20] M. M. Leivo, J. P. Pekola, and D. V. Averin, Efficient Peltier refrigeration by a pair of normal metal/insulator/superconductor junctions, Appl. Phys. Lett. **68,** 1996 (1996).

[21] A. Wallraff, D. I. Schuster, A. Blais, L. Frunzio, R.-S. Huang, J. Majer, S. Kumar, S. M. Girvin, and R. J. Schoelkopf, Strong coupling of a single photon to a superconducting qubit using circuit quantum electrodynamics, Nature (London) **431,** 162 (2004).

[22] M. Jerger, S. Poletto, P. Macha, U. Hübner, E. Il'ichev, and A. V. Ustinov, Frequency division multiplexing readout and

simultaneous manipulation of an array of flux qubits, Appl. Phys. Lett. **101,** 042604 (2012).

[23] J. P. Groen, D. Ristè, L. Tornberg, J. Cramer, P. C. de Groot, T. Picot, G. Johansson, and L. DiCarlo, Partial-Measurement Backaction and Nonclassical Weak Values in a Superconducting Circuit, Phys. Rev. Lett. **111,** 090506 (2013).

[24] M. Nahum and J. M. Martinis, Hot-electron microcalorimeters as high-resolution x-ray detectors, Appl. Phys. Lett. **66,** 3203 (1995).

[25] S. Gasparinetti, K. L. Viisanen, O.-P. Saira, T. Faivre, M. Arzeo, M. Meschke, and J. P. Pekola, Fast Electron Thermometry for Ultrasensitive Calorimetric Detection, Phys. Rev. Applied **3,** 014007 (2015).

[26] K. L. Viisanen, S. Suomela, S. Gasparinetti, O.-P. Saira, J. Ankerhold, and J. P. Pekola, Incomplete measurement of work in a dissipative two level system, New J. Phys. **17,** 055014 (2015).

[27] U. Eckern, G. Schön, and V. Ambegaokar, Quantum dynamics of a superconducting tunnel junction, Phys. Rev. B **30,** 6419 (1984).

[28] G. Schön and A. D. Zaikin, Quantum coherent effects, phase transitions, and the dissipative dynamics of ultra small tunnel junctions, Phys. Rep. **198,** 237 (1990).

[29] Fitting the base temperature data with two superimposed Lorentzians located symmetrically around zero bias yields a broadening corresponding to 31 mK.

[30] P. Lähteenmäki, V. Vesterinen, J. Hassel, H. Seppä, and P. Hakonen, Josephson junction microwave amplifier in self-organized noise compression mode, Sci. Rep. **2,** 276 (2012).

[31] Francesco Giazotto, Tero T. Heikkilä, Arttu Luukanen, Alexander M. Savin, and Jukka P. Pekola, Opportunities for mesoscopics in thermometry and refrigeration: Physics and applications, Rev. Mod. Phys. **78,** 217 (2006).

[32] P. Dubos, H. Courtois, B. Pannetier, F. K. Wilhelm, A. D. Zaikin, and G. Schn, Josephson critical current in a long mesoscopic S-N-S junction, Phys. Rev. B **63,** 064502 (2001).

[33] J. Govenius, R. E. Lake, K. Y. Tan, V. Pietilä, J. K. Julin, I. J. Maasilta, P. Virtanen, and M. Möttönen, Microwave nanobolometer based on proximity Josephson junctions, Phys. Rev. B **90,** 064505 (2014).

[34] J. Govenius, R. E. Lake, K. Y. Tan, and M. Möttönen, Detection of Zeptojoule Microwave Pulses Using Electrothermal Feedback in Proximity-Induced Josephson Junctions, Phys. Rev. Lett. **117,** 030802 (2016).

[35] Here, we refer to an experimental setting where radiation is coupled to a small absorber, and the thermometer is used to monitor the absorber temperature.

[36] K. Schwab, E. A. Henriksen, J. M. Worlock, and M. L. Roukes, Measurement of the quantum of thermal conductance, Nature (London) **404,** 974 (2000).

[37] Cabling losses on the input side are not included and will diminish the estimated dissipation proportionally.